La mer 32: 225–234, 1994
Société franco-japonaise d'océanographie, Tokyo

A numerical study on currents in the Taiwan Strait during summertime

Sen JAN*, Ching-Sheng CHERN* and Joe WANG*

Abstract : A zonal sand ridge north of the Peng-hu Channel has a strong influence on flows in the Taiwan Strait. Previous summertime hydrographic surveys in this area suggest that lighter surface waters flow over the ridge and then hug the west coast of Taiwan, while heavier bottom waters are blocked upstream of the ridge and turn northwestward along the local isobath.

A three-dimensional baroclinic ocean circulation model is used to study the above mentioned processes. Model results indicate that the flow pattern around the ridge is mainly determined by the bottom topography and the inertia effect associated with the incoming flows. Stratification upstream affects flow patterns downstream of the ridge. As surface waters flow farther north, they tend to converge eastward due to both the baroclinic effect and topographic β-effect. Meanwhile, a wave-like structure in the density field is formed downstream of the ridge. The simulated flow patterns are in close agreement with observations.

1. Introduction

The flows in the Taiwan Strait (TS) are significantly affected by the topography. Fig. 1 shows isobaths in the TS. The major topographic features, as illustrated in this figure, are the Chang-yuen ridge (CYR) north of the Peng-hu Channel (PHC), the Formosa Banks in the southwestern TS, and the deepening topography in the northeastern TS. Past observations suggest that the circulation in the Strait is dynamically complex.

Irrespective of its driving mechanisms, a permanent northeastward flow was observed through PHC to the northern TS (CHUANG, 1985, 1986; WANG *et al.*, 1987, 1988). As this flow impinges on the CYR, the surface and bottom waters will flow in different directions upstream of the CYR, at least during the summer season. Figs. 2a and 2b show isopycnals at 10 m and 50 m depths, respectively, in the TS during September 1–6, 1988. Lighter surface waters, shown in Fig. 2a, may flow over the CYR and distribute along the eastern side of the TS, while heavier bottom waters, shown in Fig. 2b, are blocked and then separated from the Taiwan coast south of the CYR. The vertical density transect at a zonal section (line B in Fig. 2a) indicates that flows are well stratified in the southern PHC, as shown in Fig. 3a. Fig. 3b shows another density transect north of the CYR (line C in Fig. 2a). The original, vertically stratified waters become uniform in the eastern TS and remain stratified in the western TS. Typically, these hydrographic patterns last from May to early September (WANG *et al.*, 1988; WANG and CHERN, 1991, 1992).

The influence of topography on stratified flows has been studied extensively (e.g., HUPPERT and STERN, 1974; MERKINE, 1975, 1976; NOF, 1978). These theoretical analyses indicated that for a rotating stratified flow over a ridge, there will be a streamwise density gradient on the upstream side of the ridge. This density gradient can support a cross-stream vertical shear through the thermal wind relation. Hence the flow will be deflected to the left in front of this ridge at least at lower layers (MERKINE, 1975). This is a possible cause for the observed vertical veering of currents in front of the CYR. However, the topography in the TS is much more complex than that of these theoretical models. The adjustment processes induced by the shoaling topography in the PHC and the blocking of the CYR can magnify nonlinear effects and make the problem analytically intractable.

* Institute of Oceanography, National Taiwan University, Taipei, Taiwan, China

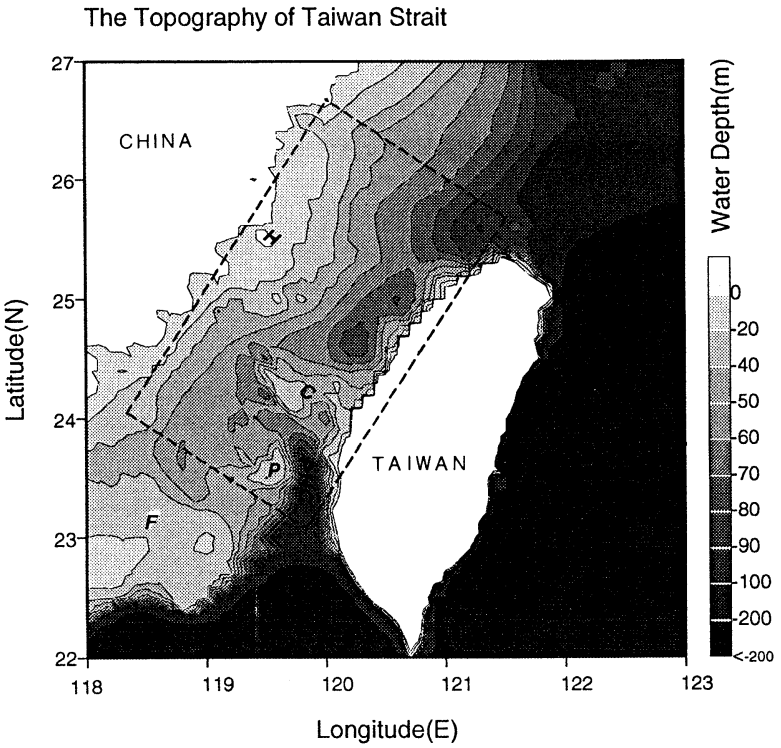

Fig. 1. Bottom topography of the Taiwan Strait, in which *F* is the Formosa Banks, *P* is the Peng-hu Islands, *PHC* is the Peng-hu Channel, *C* is the Chang-yuen ridge and *H* is Hai-tang Island. The dashed rectangle is the computation domain.

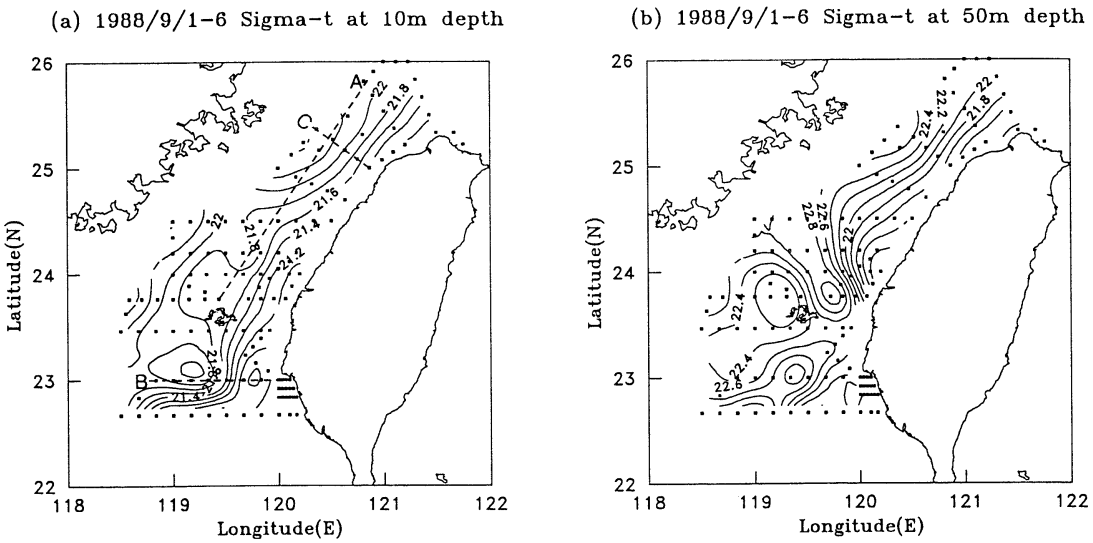

Fig. 2. Isopycnals (in σ_t) at depths 10 m and 50 m observed in the Taiwan Strait during September 1–6, 1988 (from WANG and CHERN, 1992). Dots denote locations of CTD cast.

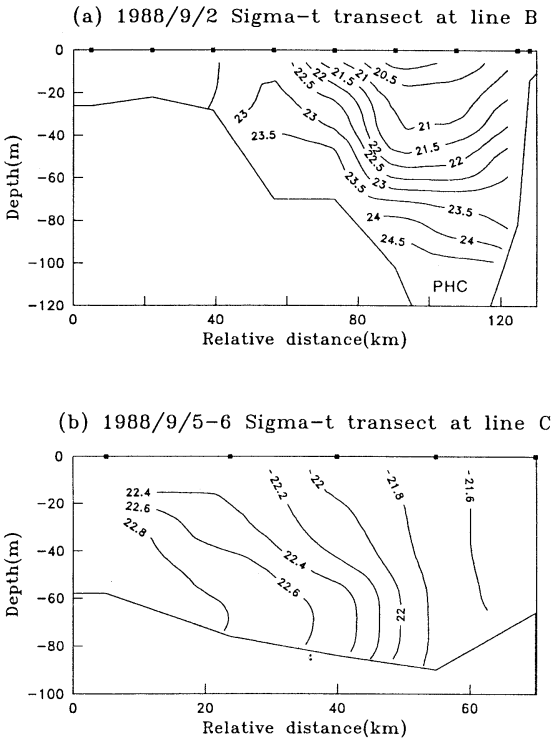

Fig. 3. Vertical density transects at lines B and C in Fig. 2.

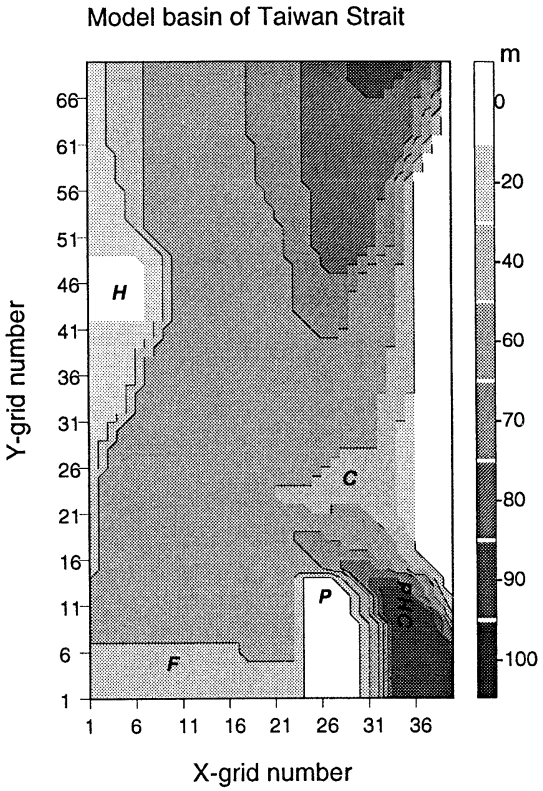

Fig. 4. Model basin of the Taiwan Strait with the same notations as in Fig. 1.

WANG and CHERN (1991) used a homogeneous, frictionless model, similar to the NOF's (1978) formulation, to study the current structure in the CYR area. They found that the Rossby number of the incoming flow is a dominant parameter affecting the flow pattern. As the Rossby number diminishes, the flow will separate from the east coast and turn northwestward. Following their study, a three-dimensional, baroclinic, ocean circulation model is used to investigate the effect of the upstream stratification on the summertime flow pattern in the TS. In order to identify the main mechanism controlling the flow field, the model ocean has a topography which resembles that of the TS. Influences of the stratification and inertia of the incoming flow are discussed.

2. Numerical model

The ocean general circulation model described by SEMTNER (1974, 1986) is used to study the summertime circulation in the TS. The dashed rectangle shown in Fig. 1 indicates our computation domain. For convenience, the x-axis is transverse to the Strait and the y-axis aligned along the Strait, which is about 32° clockwise from north. Fig. 4 shows the model basin, which retains essential features of the bottom topography of the TS. The model basin has 40 and 70 grid points in the x and y directions with a mesh size of 5 km. There are seven levels in the vertical with the level thickness being 20 m for the top three levels, reduced to 10 m for the lower four levels to better resolve the steep rise near the northern end of the PHC.

Under the Boussinesq, hydrostatic and rigid-lid approximations, the governing equations are as follows

$$\frac{Du}{Dt} - fv = -\frac{1}{\rho_0} P_x + \nu u_{zz} + A_M \nabla_H^2 u$$

$$\frac{Dv}{Dt} + fu = -\frac{1}{\rho_0} P_y + \nu v_{zz} + A_M \nabla_H^2 v$$

$$P_z = -\rho g$$

$$u_x + v_y + w_z = 0,$$

in which x, y, z form a right-handed Cartesian coordinate system with $z = 0$ at the sea surface and u, v, w are velocity components in the three directions respectively, t is time, P is pressure, ρ is density, ρ_0 is a reference density, f is Coriolis parameter, D/Dt is total time derivative, ∇_H is horizontal gradient operator, A_M and ν are horizontal and vertical eddy viscosities. For simplicity, the density diffusion equation is considered in the present model as,

$$\frac{D\rho}{Dt} = \nu\rho_{zz} + A_H\nabla_H^2\rho,$$

in which A_H is horizontal diffusivity.

Variables are calculated at the center of each grid box.

WANG and CHERN (1991) showed that the flow pattern around the CYR is mainly determined by the volume transport through the PHC. Unfortunately, there are no comprehensive current measurements in this channel. The actual transport in the PHC is still not clear. However, we can estimate the transport with current data acquired by CHUANG (1986). Since the observed near-bottom (80 m depth) flow is typically 30 cm/s northward in summer, the upper layer flow should be faster than this. Thus, a reasonable estimate of the vertically averaged velocity is 50 cm/s northward. We further assume that the current is 20 km wide and 100 m thick; a volume transport of about 1 Sv (10^6 m^3/s) is thus used to spin up the model. This value is the same as the total volume transport through the TS estimated by WYRTKI (1961). On the other hand, the observed hydrography (XIAO, 1988) shows that isotherms and isohalines on the Formosa Banks are nearly transverse to the Strait. Moreover, images of sea surface temperature and ocean color (LIU, 1993) also show that surface waters flow mostly through the PHC into the TS. The above evidences imply that the transport across the Formosa Banks is quite small. So the net transport through the southwestern boundary is specified zero.

The model ocean is quiescent and homogeneous initially. According to the density structure shown in Fig. 3a, a simplified two-layer, with a pycnocline at level 3, stratified flow is clamped at the entrance of the PHC. The northward transport in the PHC is gradually increased to 1 Sv during the first 10 days and then levels off. The zero normal gradient boundary condition for the density and horizontal velocity is imposed at the northern and southwestern open boundaries. At the rigid surface, $z = 0$,

$$\frac{\partial\rho}{\partial z} = 0, \quad w = 0, \quad \tau_s = 0,$$

in which τ_s is sea surface stress. Since the vertical level size is too coarse to resolve the bottom boundary layer, a quadratic stress law and density flux boundary conditions are used on the ocean floor, $z = -h(x, y)$,

$$\frac{\partial\rho}{\partial z} = 0,$$
$$(\tau_b^x, \tau_b^y) = C_d(u^2 + v^2)^{1/2}(u, v),$$

where τ_b is bottom stress, C_d is friction coefficient. The vertical velocity on the uneven bottom is $w = uh_x + vh_y$. The normal component of momentum and density fluxes are zeros on all solid walls. Numerical integration time step is 60 seconds and other parameters are $A_M = 2 \times 10^6$ cm^2/s, $\nu = 1$ cm^2/s, $A_H = 2 \times 10^5$ cm^2/s, and $C_d = 0.001$. In the present model, A_M and ν are assumed as small as possible provided the computation remains stable. It is hoped that this choice may reduce the frictional effect and make the model to be inertia dominant. Thus we can mainly examine the interaction between the topography and the inertia effect. In order to absorb the computational disturbances generated on the open boundary, a sponge layer is formed at 3 grid points adjacent to the northern boundary, where the horizontal eddy viscosity is 2, 4 and 8 times as large as the above A_M.

3. Model results

Two cases, SA and SB, with different stratification conditions for flows at the entrance of the PHC are considered in this study. Densities (σ_t) at levels 1 and 2, 3, and 4 to 7 at the open boundary south of the PHC are 21, 22.5 and 24 in case SA, and 21, 21.15 and 21.3 in case SB. A useful nondimensional parameter measuring stratification strength is the Burger number,

$$S = g\frac{\Delta\rho}{\rho}\frac{H}{f^2L^2},$$

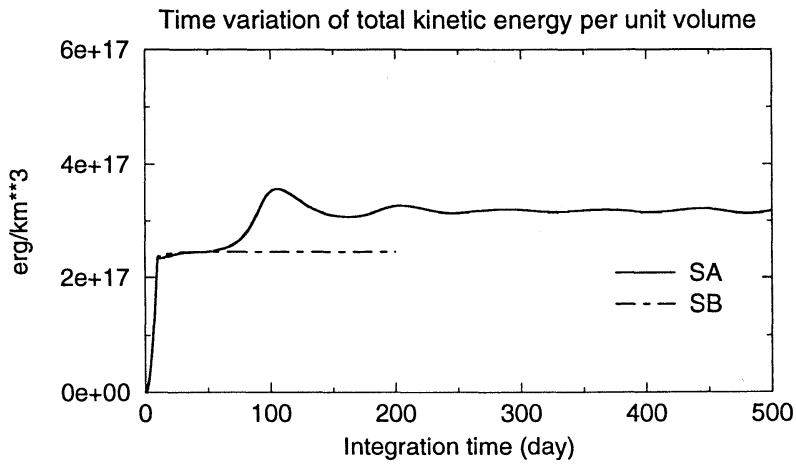

Fig. 5. Time variation of the total kinetic energy per unit volume (km^3) for cases SA and SB during the integration period.

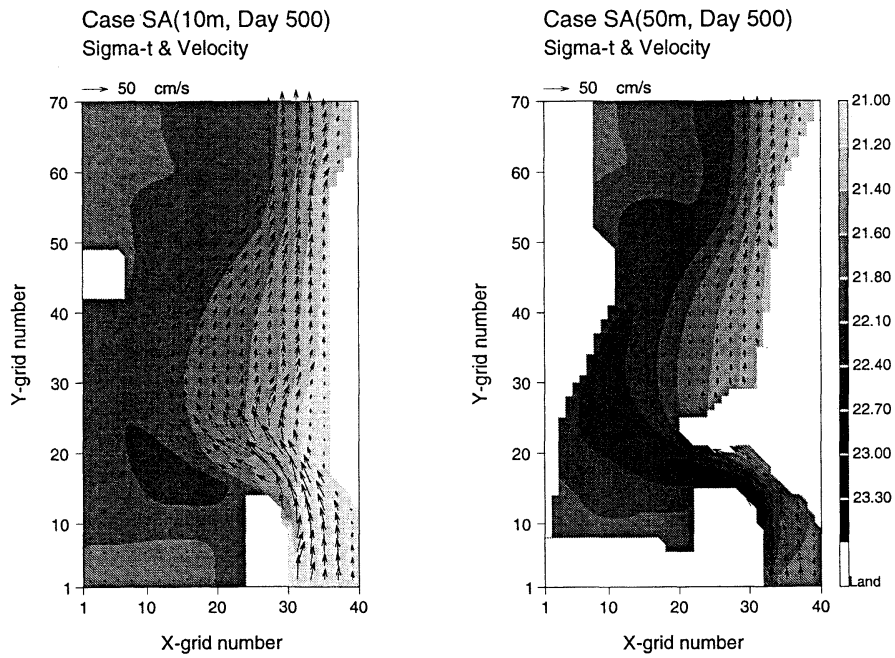

Fig. 6. Distribution of velocity and density (in σ_t) at 10 m and 50 m depths in case SA at day 500. Velocity vectors are plotted at every two grid points in both the x and y directions.

in which L is horizontal length scale of the topography rise and $\Delta\rho$ is density difference over the vertical length scale H. For fixed geometric scales, H = 60 m and L = 25 km, the Burger number is proportional to the density difference over H. So the Burger number in cases SA and SB is estimated 0.9 and 0.09, respectively, with $g = 9.8\ m^2/s$ and $f = 5.5 \times 10^{-5}\ s^{-1}$. The typical Burger number is around 1 in the PHC during summer.

Fig. 5 shows the time variation of the total kinetic energy per unit volume (km^3) during the integration period. This figure indicates that integration time needed to get a quasi-steady

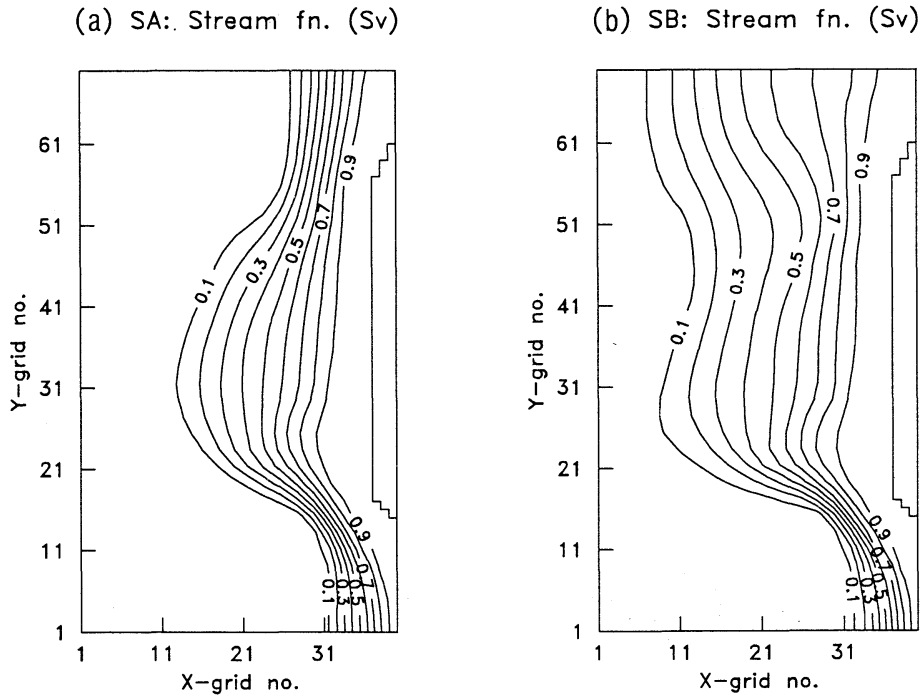

Fig. 7. Transport stream lines in cases SA and SB.

state is 350 days for SA and merely 100 days for SB. The strong baroclinicity is a possible cause for case SA to take a longer time.

There is no significant variation in flow fields after these 350 or 100 days.

Fig. 6 shows the horizontal distributions of velocity and density at 10 m (surface) and 50 m (bottom) depths in case SA at day 500. At the surface, the flow with a speed of about 25 cm/s at the entrance of the PHC is accelerated to about 50 cm/s as it reaches the northern end of the PHC. As surface waters flow over the CYR, a negative relative vorticity will be produced on the ridge due to the potential vorticity conservation associated with the shoaling topography. Thus, a stagnant region is formed in the nearshore area west of Taiwan. In the northern TS, surface flows gradually converge eastward to the Taiwan coast. The average velocity here is about 40 cm/s which is of the same order as that measured by WANG *et al.* (1988). Flows are relatively weak at the western portion of the Strait. Bottom flows, on the other hand, behave differently. The heavier waters upwelled from the lower layer of the PHC are deflected northwestward forming a cold water tongue to the northwest of the CYR. These bottom waters then flow by the western boundary to the northern TS, where the mean velocity is about 5 cm/s.

The flow pattern in the area south of the CYR in case SB is similar to that in case SA, but shows a different feature in the northern TS. Fig. 7 shows the distribution of stream lines in these two cases. In case SB, stream lines tend to move westward in the northern TS, as shown in Fig. 7; and so are isopycnals (not shown). This is inconsistent with the observed hydrography shown in Fig. 2. In case SA, however, the convergence of the transport streamlines in the northwestern TS is apparent. Theoretically, for a stratified rotating flow over a ridge, the vertical shear of the cross-stream velocity in front of the ridge depends on the upstream Burger number (MERKINE, 1975; CHERN and WANG, 1990). Since the Burger numbers in both cases are not greater than 1, the flow pattern around the CYR is determined mainly by the local Rossby number, similarly to the homogeneous case studied by WANG and CHERN (1991). However, this

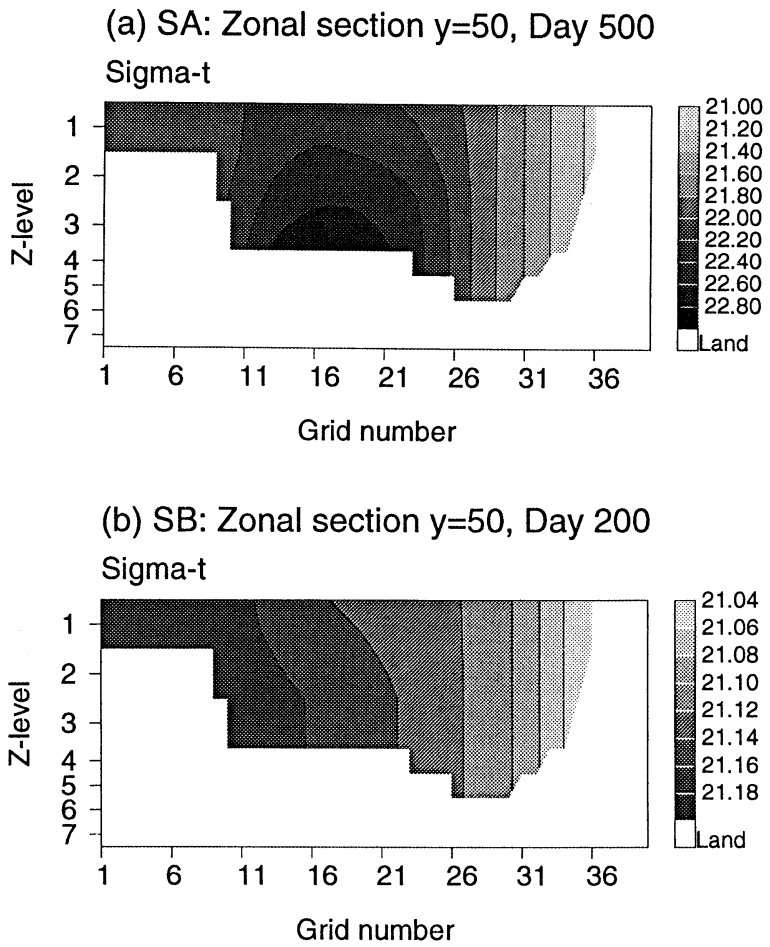

Fig. 8. Vertical density transect in cases SA and SB at the zonal section $y = 50$.

does not mean that the upstream stratification has no effect on the flow structure at all. North of the CYR, the original vertical stratification is transformed into a cross-stream density front. Fig. 8 shows vertical density transects at the zonal section $y = 50$ in cases SA and SB. Waters are vertically uniform in the eastern part and stratified in the western part of the northern TS in both cases. The thermal wind relation indicates that a larger cross-stream density gradient in case SA may induce a stronger streamwise vertical shear within the frontal region. Since this horizontal density front is in the eastern part of the northern TS, the intensification and convergence of flows here in case SA are partly due to this process. Furthermore, the deepening topography in this area relating to the topographic β-effect will also enhance the above mentioned process.

4. Discussion and concluding remarks

In addition to the mean flow pattern described in previous sections, we can also identify a wave-like structure in the density field downstream of the CYR. Fig. 9 shows density transects at the meridional section $x = 21$ in the two cases. The wave-like pattern is apparent in case SA and is relatively weak in case SB. According to model results, lighter surface waters subside immediately north of the CYR as bottom flows turn northwestward in front of this ridge. In the northern TS, the stratified waters

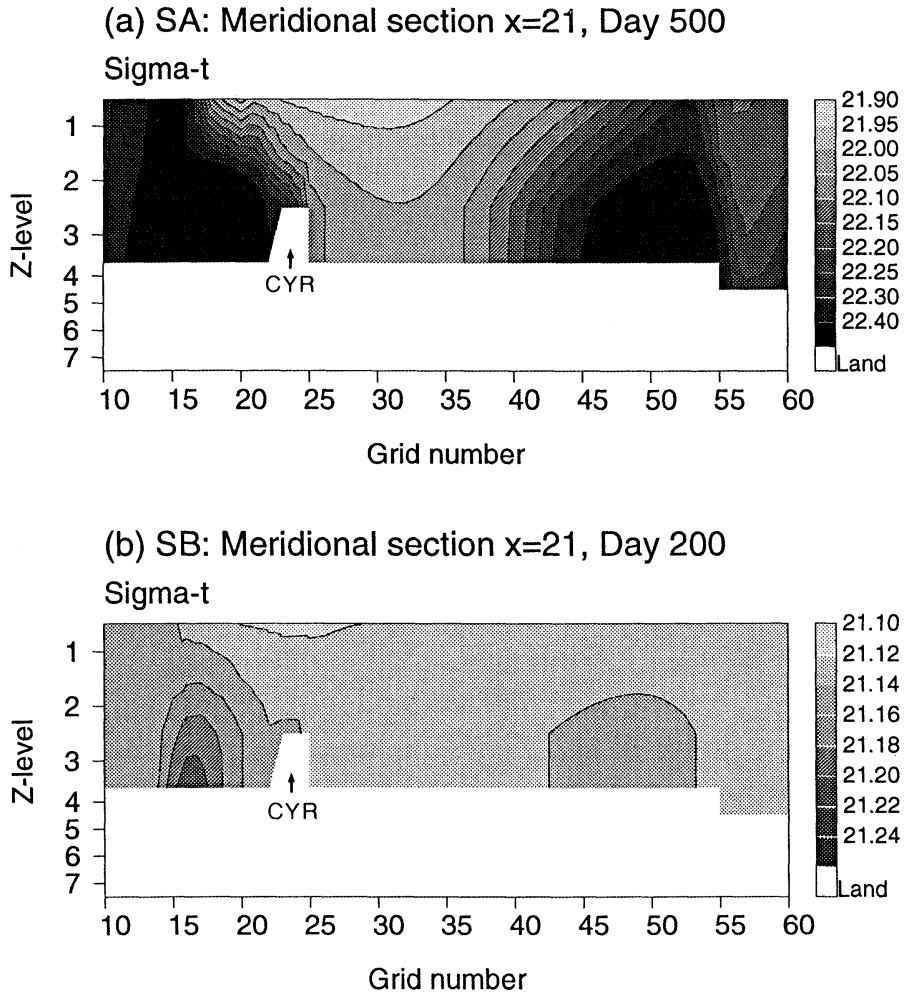

Fig. 9. Vertical density transects in cases SA and SB at the meridional section $x = 21$.

in the western portion of the Strait are pushed eastward due to the thermal wind relation and the topographic β-effect, as mentioned in a previous section. Hence, a wave-like pattern is formed in the center of the Strait. This kind of density structure has also been observed along the central line of the Strait, as shown in Fig. 10, which is the density transect at line A in Fig. 2. The resemblance of isopycnals distribution between this figure and case SA in Fig. 9 is clear. The formation of this density structure and its relation to the upstream stratified condition need further study.

Since tidal currents are strong in the Strait, the bottom Ekman layer associated with the frictional stresses may also affect the flow pattern. Different frictional coefficients have been used in our model to study this effect. With C_d increase, model results indicate that transport streamlines tend to move westward in the northern TS. However, for C_d in the range from 0.001 to 0.005, there is no appreciable difference among the modeled flow fields. Since there is insufficient information about the frictional strength in the TS, and the simulated flow patterns shown previously are in good agreement with the observed hydrography, we may say that the parameter values used in the present model are reasonable.

To summarize, this model study verifies that

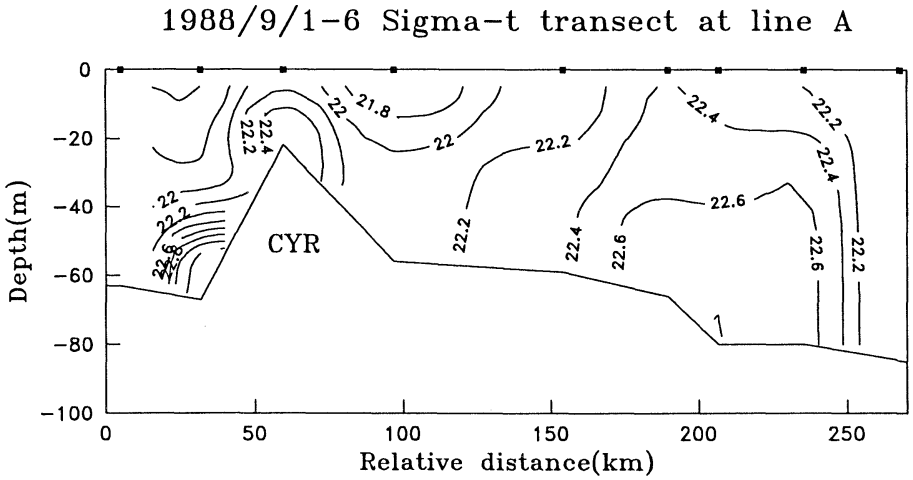

Fig. 10. Vertical density transect at line A in Fig. 2a.

the summertime flow pattern in the Strait is determined by the bottom topography, the stratification and volume transport in the southern entrance of the PHC. Due to shoaling at the northern end of the PHC, surface waters are accelerated and then flow over the ridge. Meanwhile, bottom waters are blocked south of the CYR and flow northwestward following the local isobaths. After surface and bottom waters veered in front of the ridge, original vertically stratified waters are transformed to be uniform in the eastern portion and stratified in the western portion of the northern TS. For the upstream Burger number of about 1, the above transformation related to the baroclinic effect together with the topographic β-effect can enhance downstream flows toward the Taiwan coast. In the central part of the TS, a wave-like density structure is formed north of the CYR.

References

CHERN, C.-S. and J. WANG (1990): On the Kuroshio branch current north of Taiwan. Acta Oceanogr. Taiwanica, **25**, 55–64.

CHUANG, W.-S. (1985): Dynamics of subtidal flow in the Taiwan Strait. J. Oceanogr. Soc. Japan, **41**, 65–72.

CHUANG, W.-S. (1986): A note on the driving mechanisms of current in the Taiwan Strait. J. Oceanogr. Soc. Japan, **42**, 355–361.

HUPPERT, H.E., and M.E. STERN (1974): Ageostrophic effects in rotating stratified flow. J. Fluid Mech., **62**, 369–385.

LIU, A.K. (1993): Satellite remote sensing for ocean application. Conference on Marine Meteorology Proceedings, Central Weather Bureau, Taipei, 177–188.

MERKINE, L.-O. (1975): Steady finite-amplitude baroclinic flow over long topography in a rotating stratified atmosphere. J. Atmos. Sci., **32**, 1881–1893.

MERKINE, L.-O. and K.-R. EUGENIA (1976): Rotating stratified flow over finite isolated topography. J. Atmos. Sci., **33**, 908–922.

NOF, D. (1978): On geostrophic adjustment in sea straits and wide estuaries: Theory and laboratory experiments. Part I: One-layer system. J. Phys. Oceanogr., **8**, 690–702.

SEMTNER, A.J. (1974): An oceanic general circulation model with bottom topography. Numerical simulation of weather and climate. Tech. Rep. 9, Dept. of Meteorology, UCLA, 99 pp.

SEMTNER, A.J. (1986): Finite difference formulation of a world ocean model. Proceedings of the NATO Advanced Study Institute on Advanced Physical Oceanographic Numerical Modelling, ed. J. J. O'BRIEN, D. Reidel Publishing Co., Dordrecht.

WANG, J. and C.-S. CHERN (1991): Some aspects on flow-topography interactions in the Taiwan Strait. A process study of subtidal flows on Chang-yuen ridge. International Symposium on Marine Pollution in Celebration of the 60th Anniv. of National Cheng-Kung Univ., 55–67.

WANG, J. and C.-S. CHERN (1992): On the distribution of bottom cold waters in Taiwan Strait during summertime. La mer, **30**, 213–221.

WANG, J., C.-S. CHERN, C.-H. CHEN and Y.-Y.

HUANG (1987): Oceanographic observations and a diagnostic system at the CBK area. Special Pub. No. 53, Institute of Oceanography, National Taiwan University. 192 pp. (in Chinese)

WANG, J., C.-S. CHERN, C.-H. CHEN and Y.-Y. HUANG (1988): Oceanographic observations at CBK-11 area platform and the nearby area. Special Pub. No. 57, Institute of Oceanography, National Taiwan Uuiversity, 279 pp. (in Chinese)

WYRTKI, K. (1961): Physical oceanography of the southeast Asia waters. Scientific results of marine investigations of the South China Sea and Gulf of Thailand, 1959-1961, Naga Report, **2**, 195 pp.

XIAO, H. (1988): Studies of coastal upwelling in western Taiwan Strait. J. Oceanogr. in Taiwan Strait, **7**, 135-142.